Biosensors and Bioelectronics 129 (2019) 139–146

Contents lists available at ScienceDirect

Biosensors and Bioelectronics

journal homepage: www.elsevier.com/locate/bios

Fabrication of pioneering 3D sakura-shaped metal-organic coordination polymers Cu@L-Glu phenomenal for signal amplification in highly sensitive detection of zearalenone

Xingduo Ji[a,1], Chao Yu[b,1], Yilin Wen[b], Jun Chen[b], Yujie Yu[a], Chengli Zhang[b], Rufei Gao[a], Xinyi Mu[a], Junlin He[a,*]

[a] School of Public Health and Management, Chongqing Medical University, Chongqing 400016, People's Republic of China
[b] College of Pharmacy, Chongqing Medical University, Chongqing 400016, People's Republic of China

ARTICLE INFO

Keywords:
3D sakura-shaped
Signal amplification
ZEN detection
Electrochemical aptasensor

ABSTRACT

Low molecular weight pollutants from foods have aroused global attention due to their toxicity after long-time exposure. There is an increased demand for appropriate methods to detect these pollutants in foods. In this study, a brand-new type of nano metal–organic coordination polymers (MOCPs) nanocarriers (3D sakura-shaped copper (II) ions@L-glutamic acid (L-Glu)) has been first synthesized. We herein demonstrate a facile chelated method that allows the combination of copper (II) ions and L-Glu. A series of controlled experiments have revealed that the reaction time and the ratio of reactants played the crucial roles in affecting the morphology of the final product. 3D sakura-shaped Cu@L-Glu combined with palladium-platinum nanoparticle (Pd-PtNPs) to obtain Cu@L-Glu/Pd-PtNPs acting as the signal tag, which applied in electrochemical aptasensor for ultrasensitive detection of zearalenone (ZEN). A glassy carbon electrode was first modified with spherical Au-PANI-Au nanohybrids to enhance the conductivity and immobilize more amino modified ZEN aptamer. Cu@L-Glu/Pd-PtNPs were labeled with Complementary DNA (partial matching with ZEN aptamer) to form bioconjugates for signal amplification. After the hybridization reaction of ZEN aptamer and the bioconjugates, a significant electrochemical signal from the catalysis of H_2O_2 by Cu@L-Glu/Pd-PtNPs can be observed. ZEN competed with bioconjugates for binding to ZEN aptamer, resulting in decreased the electrochemical signal. Chronoamperometry was applied to record the final electrochemical signals. Under optimal conditions, the electrochemical aptasensor exhibited desirable sensitive detection of ZEN with a wide linearity ranging from 1 fg/mL to 100 ng/mL and a relatively low detection limit of 0.45 fg/mL (S/N = 3). Furthermore, the proposed electrochemical aptasensor shows excellent selectivity to the ZEN in the presence of possible interfering substances, and has potential application for ZEN detection in food samples.

1. Introduction

Zearalenone (ZEN), as an estrogenic mycotoxin, is secondary metabolites produced by several species such as Fusarium graminearum and Fusarium culmorum (Bennett and Klich, 2003; Richard, 2007; Zhang et al., 2018b). ZEN is found in corn, wheat, beer, and it considered to be one of the most common contaminants in grains (Liu et al., 2014; Zaied et al., 2012). Since ZEN might cause adverse effects on humans and animals, including teratogenesis, abortion, hepatotoxicity, hematological toxicity and carcinogenicity (Schneider and Dickert, 1994; Zinedine et al., 2007). The International Agency for Research on Cancer has classified ZEN as group III carcinogen (Zhang et al., 2017). There is an urgent need for the innovation and development of monitoring systems to monitor the quality of grains. At present, High-performance liquid chromatography (Chen et al., 2017a), liquid chromatography-mass spectrometry (Njumbe Ediage et al., 2015) and enzyme-linked immunosorbent assay (ELISA) (Ghali et al., 2008) are the traditional techniques utilized for ZEN determination. Although these assay methods show good specificity and accuracy, they have limited sensitivity and require expensive instruments (Hervas et al., 2010). Recently, electrochemical techniques have been developed for ZEN detection, which have cost-effective, remarkable sensitivity and specificity (Hervas et al., 2009).

Aptamers are synthetic single-stranded DNA or RNA molecules with

* Correspondence to: Chongqing Medical University, 1 Yi Xue Yuan Road, Box 197#, Yuzhong District, Chongqing 400016, People's Republic of China.
E-mail address: hejunlin@cqmu.edu.cn (J. He).
[1] Chao Yu and Xingduo Ji contributed equally to this work.

https://doi.org/10.1016/j.bios.2019.01.012
Received 5 October 2018; Received in revised form 11 December 2018; Accepted 4 January 2019
Available online 15 January 2019
0956-5663/

high specificity and target binding affinity (Cho et al., 2009). And in comparison to antibodies, aptamers are easy to synthesize and have low production cost (Schmidt et al., 2004), which is particularly suitable for large applications of low molecular weight pollutants recognition. Thus, the aptamers are used extensively for electrochemical biosensor. Small molecule toxins, small molecule antigens and haptens are not available for sandwich assays because of the lack of more than two sites that can be used as sandwich methods. The detection of small molecules (such as ZEN) is better conducted using an indirect competition format which can provide higher sensitivity and selectivity than the direct method (Kong et al., 2017; Xu et al., 2017). Therefore, the development of the indirect competition assay combine with aptamers for the sensitive detection of ZEN is highly desirable.

To achieve signal amplification of the electrochemical aptasensor, palladium nanoparticles (PdNPs) and platinum nanoparticles (PtNPs) were used as a signal enhancer. PdNPs and PtNPs have an excellent biocompatibility with biomolecules (Li et al., 2017b) and significantly well electrocatalytic activity (Singhal et al., 2017). Pd-PtNPs have stronger catalytic activity to H_2O_2 than the PdNPs or PtNPs due to adding of the second metal elements can change the electronic structure and further tune the adsorption intensity of reactive molecules (Deng et al., 2012).

However, metal nanoparticles tend to aggregate in catalytic processes due to their high surface energy (Yan et al., 2018). To avoid aggregation, diverse supports have been utilized to stabilize nanoparticles including one-dimensional (1D), two-dimensional (2D) and three-dimensional (3D) nanomaterials (Qin et al., 2016). Among these supports, 3D structures (such as nanoflower) as higher organized structures (Joshi and Schneider, 2012) has a higher surface-to-volume ratio (Lee et al., 2015) and can load more signal enhancers, further improving the sensitivity of the electrochemical sensor. Recently, Metal (Fang et al., 2018), metal oxide (Kong et al., 2018), transition metal dichalcogenides (Singha et al., 2018), metal-organic coordination polymers (MOCPs) (Hanifehpour et al., 2015) and carbon based nanomaterials (Du et al., 2014) have been developed to form 3D flower-like nanostructures. Nanometer-sized particles of MOCPs, as an organic-inorganic hybrids material, have gained significant attention due to their application in many fields such as catalysis (Wang et al., 2011a), luminescence (Mahmoudi and Morsali, 2009), drug delivery (Ma and Moulton, 2011) and biosensing (Fu et al., 2011). Specially, the MOCPs containing copper(II) ions show promising application prospects because of their ease of synthesis, excellent physical and chemical properties (Lin et al., 2014; Masoomi and Morsali, 2013). The selection of proper organic ligands can affect the ultimate self-assembling process and structures of the target copper (II) ions MOCPs (Lin et al., 2014). L-Glu as an organic ligand (Zhou et al., 2014) has good biocompatibility and contains amino group and carboxyl group, wherein carboxyl oxygen could chelate almost all metal ions in oxidation state (ElShafei et al., 2010). Fortunately, we pioneer choose copper (II) ions and L-Glu as reagents to synthesize brand-new 3D sakura-shaped Cu@L-Glu MOCPs which could serve as an excellent platform for loading more signal enhancers. The resultant Cu@L-Glu/Pd-Pt nanocomposites exhibited excellent properties and contributed to the performance of the aptasensor.

Meanwhile, immobilization of the biomolecules on the electrode is also crucial for the sensitivity and stability of electrochemical aptasensor. A variety of nanomaterials have been utilized for the electrode modification material, such as carbon nanomaterials, noble metal nanoparticles, quantum dots and conducting polymers. Polyaniline (PANI), as one of conductive polymers, has been widely investigated due to easy synthesis, low cost, high controllable conductivity and good electrochemical properties (Chen et al., 2017b; Wu et al., 2018). Gold nanoparticles (AuNPs) are high conducive nanomaterials, which have good biological compatibility (Wei et al., 2011) and have been applied widely in biosensor field (Fan et al., 2015). The incorporation of AuNPs into PANI can further improve performances of PANI. Presently, diverse nanostructures of Au-PANI have been synthesized and used in the fabrication process of electrochemical biosensors which shows excellent sensitivity (Wang et al., 2011b). L Yang et al. synthesized core-shell Au-PANI nanohybrids, PANI as a protective shell not only has good biocompatibility, but it avoids the aggregation of nanoparticles (Li et al., 2017a). In order to immobilize more biorecognition elements, AuNPs were loaded on the surface of PANI shell of core-shell structure Au-PANI. In this work, we prepared spherical Au-PANI-Au nanohybrids by one-step method, which could combine a large number of the amino group labeled aptamer (AP) through strong Au-NH_2 bonds (Zhang et al., 2018a), which further improved the sensitivity of the aptasensor.

Herein, a novel electrochemical aptasensor with highly sensitive and selective was constructed for the quick detection of ZEN. L-Glu with carboxyl group and amino group was used as precursor for the copper (II) ions nanocrystals to obtain 3D sakura-shaped Cu@L-Glu MOCPs for the first time in this study. 3D sakura-shaped of nanomaterial served as an excellent platform to avoid the aggregation of Pd-PtNPs. Meanwhile, more signal enhancers were loaded on the 3D sakura-shaped Cu@L-Glu MOCPs surface to amplify the electrochemical signals and thus increase the sensitivity of aptasensor. The resultant Cu@L-Glu/Pd-Pt nanocomposites were used to label the complementary DNA (CP), which could catalyze the reduction of H_2O_2, amplifying the detection signal. In the presence of ZEN, a significant reduction can be observed in signal because of ZEN competed with bioconjugates for binding to ZEN aptamer (AP) forming ZEN-ZEN aptamer complex. In addition, spherical Au-PANI-Au nanohybrids were used to modify the electrode, which further improved the sensitivity of the electrochemical aptasensor. This proposed electrochemical aptasensor showed excellent analytical performance for ZEN, indicating its great potential for rapid and accurate ZEN determination.

2. Experimental

2.1. Materials and chemicals

ZEN standard solution was purchased from Toronto Research Chemicals Inc. (Toronto, Canada, www.trc-canada.com). ZEN ELISA kit was obtained from Hebei Elisa Biotechnology Co., Ltd. (Hebei, China, www.hbelisa.com). Gold (III) chloride trihydrate ($HAuCl_4{\cdot}4H_2O$), chloroplatinic acid ($H_2PtCl_6{\cdot}6H_2O$), sodium tetrachloropalladate (II) (Na_2PdCl_4), 6-mercapto-1-hexanol (MCH) and tris (2-carboxyethy) phosphine hydrochloride (TCEP) were obtained from Sigma-Aldrich (St. Louis, USA, www.sigmaaldrich.com). Potassium ferricyanide ($K_3Fe(CN)_6$) and potassium ferrocyanide ($K_4Fe(CN)_6$) were supplied by Beijing Chemical Reagents Company (Beijing,China). $NaBH_4$, H_2O_2, aniline, citric acid monohydrate, cupric (II) chloride dihydrate ($CuCl_2{\cdot}2H_2O$) and L-glutamic acid (L-Glu) were purchased from Chongqing Chuandong Chemical Group Co., Ltd. (Chongqing, China). DNA oligonucleotides were synthesized and purified by Sangon Biotech Co., Ltd. (Shanghai, China).

The buffer solutions involved in this work were: 1 × TAE buffer (10 mM trishydroxymethylaminomethane hydrochloride (Tris-HCl) and 1.0 mM ethylenediaminetetraacetic acid (EDTA), pH 8.0). The Immobilization buffer (10 mM Tris-HCl, 1 mM EDTA and 0.1 M NaCl, pH 7.4) was used to diluted the AP. The hybridization buffer (10 mM Tris-HCl, 10 mM TCEP, 1 mM EDTA, 0.1 M NaCl and 5 mM $MgCl_2$, pH 7.4) was used to diluted the CP. All other reagents were analytical reagent grade and used without further purification. Ultrapure water (> 18.2 MΩ cm) obtained from a Millipore Mill-Q purification system was utilized throughout the experiment.

2.2. Apparatus and characterization

Electrochemical experiments were carried out on a CHI660D electrochemical workstation at room temperature (Chenhua Instruments Co., Shanghai, China). The morphology of different nanomaterials was

analysed using field emission scanning electron microscopy (FE-SEM, Oxford x-max50 microscope) and transmission electron microscopy (TEM, Hitachi Limited, Japan). Atomic force microscope (AFM) images were recorded by a Bruker Dimension Icon microscope (USA). X-ray photoelectron spectroscopy (XPS) was detected using a VG Scientic ESCALAB 250 spectrometer (Thermoelectricity Instruments, USA). Energy dispersive X ray spectroscopy (EDS) measurements were performed with an Oxford x-max50 microscope. UV–vis absorption spectra was recorded by a UV-2450 spectrophotometer (Shimazu, Japan). Fourier transform infrared (FT-IR) was executed using a Nicolet 6700 FT-IR spectrometer (Thermo Nicolet, USA). Zeta potential was executed using a Zetasizer Nano ZS (ZEN3600, Malvern Instruments Ltd., UK).

2.3. Preparation of Au-PANI-Au and Au-PANI nanohybrids

The Au-PANI-Au was prepared based on a previous report with slight modification (Sajanlal et al., 2008). Briefly, 31.66 mg citric acid monohydrate was dissolved in 35 mL of ultrapure water. The solution was kept at 80 °C and 170 µl of 5% $HAuCl_4$ was added. When the color of mixture changed from pale yellow to pink, 100 µl aniline was added. Subsequently, 125 µl of 5% $HAuCl_4$ was added to this solution after reacting at 80 °C for 2 min, followed by heating 5 min. This mixture solution was kept at room temperature for 2 h. Finally, the obtained Au-PANI-Au was purified by centrifugation and washed with ultrapure water and the product was dried in a vacuum oven overnight.

For proving secondary addition of $HAuCl_4$ was reduced on the surface of core-shell Au-PANI to form spherical Au-PANI-Au. The core-shell Au-PANI were synthesized using a similar method as the Au-PANI-Au nanohybrids preparation, except that 125 µl of ultrapure water was replaced with 125 µl of 5% $HAuCl_4$.

2.4. Preparation of 3D sakura-shaped Cu@L-Glu MOCPs

Ligands with lone pair electrons (such as N, O) could form two or more coordinate bonds with metal ions containing empty orbitals and further form a coordination compound with a cyclic structure by analyzing the mechanism of metal ion chelation reaction. Divalent metal ions can form metal chelates with ligands having amino groups and carboxyl groups. The copper (II) ions were chosen to chelate with L-Glu rich in carboxyl and amino groups. To prepare 3D sakura-shaped Cu@L-Glu MOCPs, 10 mg $CuCl_2{\cdot}2H_2O$ and 10 mg L-Glu were dispersed in 5 mL of phosphate buffered saline (PBS, 0.1 M, pH 8.0) with stirring at 300 rpm for 12 h. Subsequently, the obtained solution was purified by centrifugation and washed with ultrapure water three times, followed by dispersal in 1 mL of ultrapure water for further use. The preparation process of the 3D sakura-shaped Cu@L-Glu MOCPs is displayed in Scheme 1A.

3D nanostructure had a higher surface-to-volume ratio (Lee et al., 2015) and could load more Pd-PtNPs, further amplifying the signals. The reaction time and the reactants ratio had been reported for influencing the final morphologies (3D nanostructure) of MOCPs (Masoomi and Morsali, 2013). For exploring the influence of reaction time and mass ratio of $CuCl_2{\cdot}2H_2O$ and L-Glu on the morphology of Cu@L-Glu MOCPs, the reaction time and the mass ratio of $CuCl_2{\cdot}2H_2O$ and L-Glu were changed to 6 h and 24 h, 1:2 and 1:3, respectively, while keeping the other conditions constant to obtain Cu@L-Glu MOCPs.

2.5. Preparation of Pd-PtNPs, PdNPs, PtNPs

To achieve signal amplification of the electrochemical aptasensor, Pd-PtNPs were used as a signal enhancer. Pd-PtNPs were prepared as follows. Briefly, 90 µl of H_2PtCl_6 (5%) and 119 µl of Na_2PdCl_4 (5%) was added to 10 mL of ultrapure water ($n(Pt^{2+}+Pd^{2+}) = 28.89$ µmol). Then 10 mL of $NaBH_4$ solution (0.28 mg/mL) was slowly added to the complex solution with stirring at 400 rpm for 1 h. After that, the mixture solution was centrifuged at 14,000 rpm and washed repetitively with ultrapure water and ethanol three times. The final preparation was dispersed in the 2 mL of ultrapure water for further use. The details of the preparation of the PdNPs and PtNPs can be found in Supplementary information (S1).

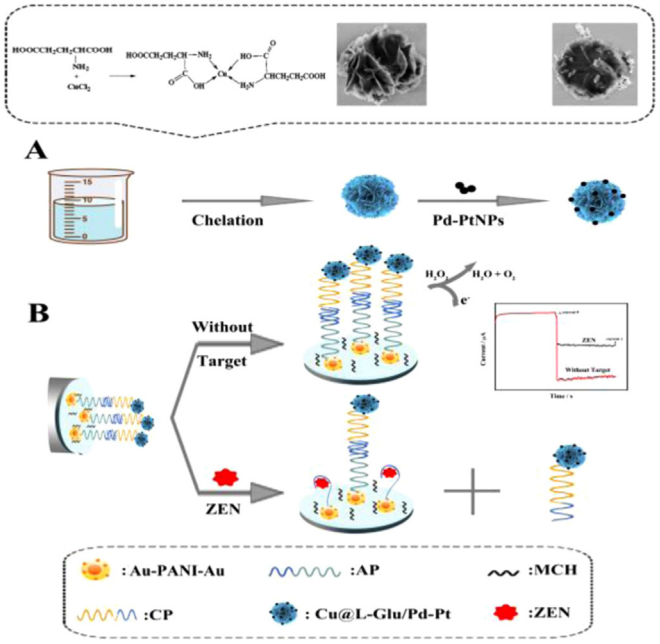

Scheme 1. (A) Preparation process of Cu@L-Glu/Pd-PtNPs. (B) Scheme of the electrochemical aptasensor fabrication.

2.6. Preparation of Cu@L-Glu/Pd-PtNPs, Cu@L-Glu/PdNPs, Cu@L-Glu/PtNPs

The 3D sakura -shaped Cu @ L-Glu MOCP with high specific surface area and rich amino group could be served as an excellent platform for in-situ assembly of Pt-PdNPs. The nanocomposites of the Cu@L-Glu and Pt-PdNPs were prepared by dissolving it in the ratio of 1: 20 in 2 mL of ultrapure water and stirred continuously for 12 h at 300 rpm. Subsequently, the prepared black solution was centrifuged at 6000 rpm for 3 min and washed with ultrapure water three times, and the resultant Cu@L-Glu/Pd-PtNPs was dispersed in 1 mL of ultrapure water for further use. The Cu@L-Glu/PdNPs and Cu@L-Glu/PtNPs were synthesized using a similar process for Cu@L-Glu/Pd-PtNPs, except that Pd-PtNPs were displaced by PdNPs and PtNPs, respectively. The preparation process of the Cu@L-Glu/Pd-PtNPs is displayed in Scheme 1A.

2.7. Preparation of Cu@L-Glu/Pd-PtNPs-CP

First of all, the disulfide bonds of CPs were reduced by TCEP in the dark for 2 h at room temperature before using. Then, 1 mL of a prepared Cu@L-Glu/Pd-PtNPs was mixed with 200 µl of 4 µM thiol-modified CP and stirred gently at 4 °C for 12 h. Subsequently, Cu@L-Glu/Pd-PtNPs-CP bioconjugates were centrifuged at 8000 rpm for 5 min and washed with hybridization solution, the obtained Cu@L-Glu/Pd-PtNPs-CP bioconjugates were then dispersed in 1 mL hybridization solution and stored at 4 °C before use.

2.8. Fabrication of electrochemical aptasensor

The fabrication process of electrochemical aptasensor is illustrated in Scheme 1. Prior to the modification, glassy carbon electrode (GCE, 4 mm in diameter) was polished with 0.3 and 0.05 µm alumina powder sequentially, and followed sonication in ultrapure water, ethanol and ultrapure water for 3 min. Then, the electrode was dried at room

temperature and modified with 10 μl of the Au-PANI-Au nanocomposite. After drying at room temperature, 10 μl of AP (2 μM) was immobilized onto the modified electrode at 37 °C for 1.5 h and AP combined with AuNPs via Au-NH_2 bonded. After that, the modified electrode was washed with ultrapure water followed by blocking 0.25 mM MCH for 30 min at room temperature to prevent nonspecific adsorption. Subsequently, 10 μl of the prepared Cu@L-Glu/Pd-PtNPs-CP bioconjugates were dropped onto the electrode to hybridize with AP for 2 h achieving signal amplification. After hybridization of AP and CP, the modified electrode was washed with ultrapure water and the aptasensor was prepared for electrochemical analysis. The process for the fabrication of electrochemical aptasensor is displayed in Scheme 1B.

2.9. Measurement procedure

Before measurement, the aptasensor was incubated with various concentrations of ZEN for 2 h at 37 °C. ZEN competed with Cu@L-Glu/Pd-PtNPs-CP bioconjugates for binding to ZEN aptamer, forming ZEN-ZEN aptamer complex and resulting in decreased the electrochemical signal. Then the aptasensor was rinsed with ultrapure water. Subsequently, amperometric i-t curve was recorded at −0.4 V in 5 mL of PBS (pH 7.4) with 20 μl of H_2O_2 (2.2 mmol/L) adding to the solution and the current changes were recorded. The change of current was obtained according to the following equation:

$$\Delta current = current1 - current0$$

where current1 is the current when different concentrations of ZEN and 20 μl of H_2O_2 (2.2 mmol/L) were added, the current0 is the background current. In Scheme 1B, the illustration was used to explain this equation.

3. Results and discussion

3.1. Characterization of the Au-PANI-Au nanohybrids

The structure and morphology of as-prepared materials were identified by TEM and FESEM. As TEM images of shown in Fig. 1A, Au-PANI was presented with a typical core-shell structure and the diameters of approximately 100 nm, a continuous and smooth shell can be observed on the surface of the core (vignette of Fig. 1A). After the reduction of $HAuCl_4$, a dense coverage of AuNPs were assembled on the surface of the core-shell Au-PANI showing spherical Au-PANI-Au had been successfully synthesized (Fig. 1A). Fig. 1D give typical FE-SEM images of Au-PANI-Au which was regular spherical morphology. The synthesis of Au-PANI-Au was further confirmed by UV–vis absorption spectra (Fig. S3A) and FT-IR spectra (Fig. S3B). As shown in Fig. S3A, for the aniline (curve a), the peak at 234 nm and 285 nm resulted from the π-π* transition of the benzenoid rings. For the Au-PANI-Au nanohybrids (curve b), three absorption peaks were observed. The π-π* transition of the benzenoid rings shifted to 215 nm and the peak at 340 nm was from the polaron/bipolaron transition (Boomi et al., 2014). The peak at 570 nm was related to the characteristic peak of AuNPs due to the surface plasmon resonance characteristics of AuNPs (Haiss. et al., 2007). Fig. S3B represented the FT-IR spectra of aniline and Au-PANI-Au nanohybrids. For the aniline (curve a), the peak at 3353.83 cm^{-1} was assigned to the N-H stretching mode, the peaks at 1620.62 cm^{-1} and 1498.62 cm^{-1} were corresponding to the C=C stretching of quinonoid and benzenoid rings (Boomi et al., 2014). For the Au-PANI-Au nanohybrids (curve b), the peak positions were different from aniline due to the interaction of AuNPs with PANI matrix. All the above results indicated that the Au-PANI-Au had been successfully synthesized.

Furthermore, the Au-PANI-Au was analysed by EDS and XPS. As shown in Fig. 2A, there were significant peaks corresponding to Au, N, C and O in the EDS image. XPS was used to characterize the synthesized Au-PANI-Au. As shown in Fig. 2B, the characteristic peaks for the Au4f, C1s, N1s and O1s were clearly observed in the Au-PANI-Au from the XPS image. The spectrum of Au4f and N1s were displayed in Fig. 2C and D. These results revealed that the Au-PANI-Au nanohybrids was successfully synthesized.

3.2. Characterization of the Cu@L-Glu and Cu@L-Glu/Pd-PtNPs

The size and morphology of the Cu@L-Glu and Cu@L-Glu/Pd-PtNPs were investigated using TEM and FE-SEM. Fig. 1B and Fig. 1E showed

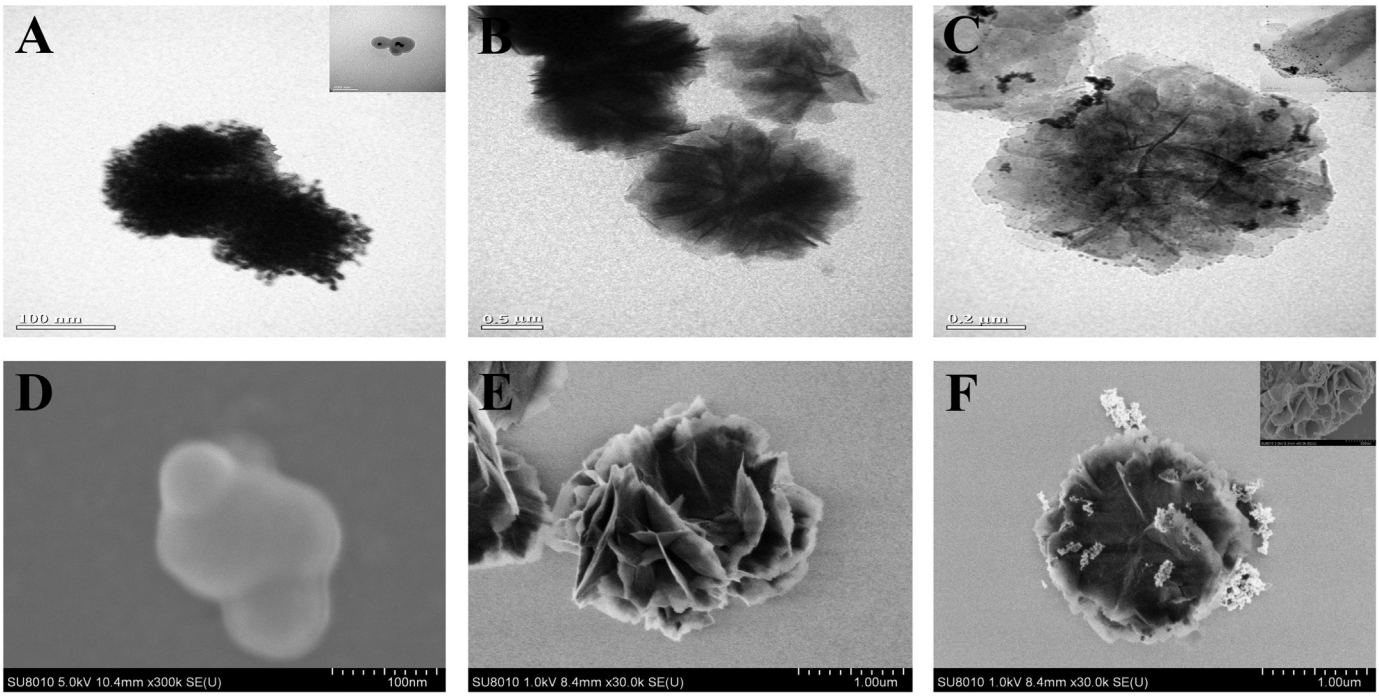

Fig. 1. TEM images of different nanohybrids: (A) Au-PANI-Au nanohybrids, (B) Cu@L-Glu MOCPs and (C) Cu@L-Glu/Pd-PtNPs. FE-SEM images of different nanomaterials: (D) Au-PANI-Au nanohybrids, (E) Cu@L-Glu MOCPs and (F) Cu@L-Glu/Pd-PtNPs.

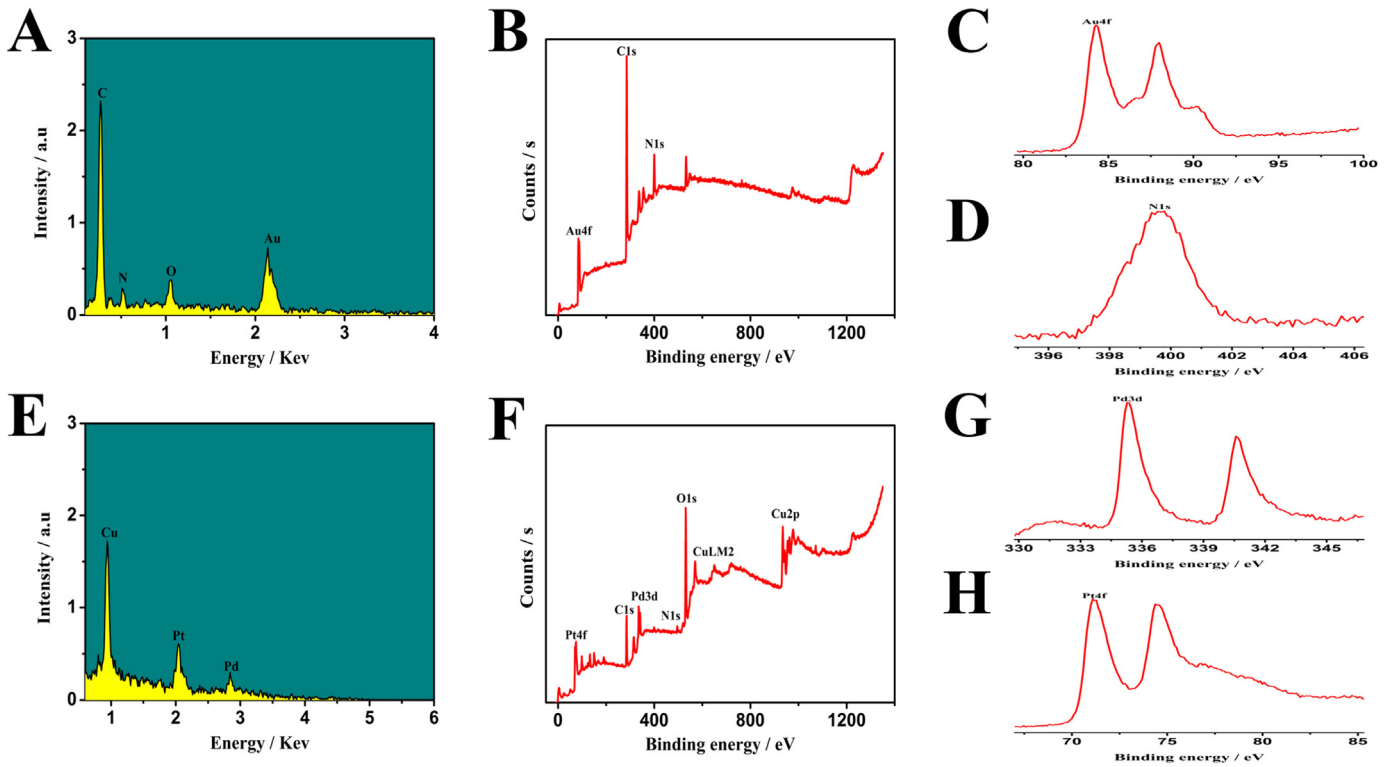

Fig. 2. The EDS spectra of (A) Au-PANI-Au nanohybrids and (E) Cu@L-Glu/Pd-PtNPs; (B) XPS spectra of Au-PANI-Au nanohybrids; XPS analysis for Au4f (C) and N1s (D) core levels of Au-PANI-Au nanohybrids; (F) XPS spectra of Cu@L-Glu/Pd-PtNPs. XPS analysis for Pd3d (G) and Pt4f (H) core levels of Cu@L-Glu/Pd-PtNPs.

the overall morphology of Cu@L-Glu. The Cu@L-Glu exhibited smooth and continuous surface with some crumpled morphologies and showed dispersed sakura-like structure with a diameter from 1 to 2 μm. Moreover, the FE-SEM images of the other Cu@L-Glu (different reaction times and different mass ratios of $CuCl_2{\cdot}2H_2O$ and L-Glu) were exhibited in Fig. S1 and Fig. S2. After the Cu@L-Glu was modified with Pd-PtNPs, a large number of bright dots was uniformly distributed on the surface of Cu@L-Glu nanoflower (Fig. 1C and Fig. 1F), suggesting the successful synthesis of Cu@L-Glu/Pd-PtNPs. Subsequently, Typical FT-IR spectra characterization (Fig. S3C) was performed for the confirmation of the Cu@L-Glu/Pd-PtNPs. For the L-Glu (curve a), the absorption peak at 3062.11 cm^{-1} were attributed to the asymmetric stretching bands of NH (Pu et al., 2012), the absorption peak at 1521.86 cm^{-1} and 1421.54 cm^{-1} were attributed to the asymmetric and symmetric absorptions of COO^- (Pu et al., 2012). For the Cu@L-Glu (curve b), the asymmetric and symmetric absorptions of COO^- disappear. The asymmetric stretching band of NH at 3062.11 cm^{-1} shifted to higher wavenumbers (3472.64 cm^{-1}) and the symmetric stretching band of NH disappeared suggesting the amino N atom was coordinated to the Cu^{2+}. After Pd-PtNPs were loaded on Cu@L-Glu (curve b), the asymmetric stretching band of NH at 3472.64 cm^{-1} further shifted to 3489.75 cm^{-1}. Meanwhile, to confirm the synthesis processes the zeta potentials of Pd-PtNPs, Cu@L-Glu and Cu@L-Glu/Pd-PtNPs were revealed in Fig. S3D. The potential of the Pd-PtNPs, Cu@L-Glu and Cu@L-Glu/Pd-PtNPs were 4.09, −18.8 and −8.99, respectively. FT-IR spectroscopy and the zeta potential both indicated that Cu@L-Glu/Pd-PtNPs were successfully synthesized.

The corresponding EDS showed the peaks of Cu, Pd and Pt elements (Fig. 2E) and the EDS mapping images of Cu, Pd and Pt were shown in Fig. S4, further confirming the formation of Cu@L-Glu/Pd-PtNPs. In addition, the Cu@L-Glu/Pd-PtNPs were analysed by XPS and the result was shown in Fig. 2F. The Cu2p, CuLM2, Pd3d, Pt4f, N1s, C1s and O1s peaks were observed, which proved Cu@L-Glu/Pd-PtNPs composites were successfully synthesized. Moreover, the Pd3d core level and Pt4f core level suggested that the Cu@L-Glu/Pd-PtNPs effectively anchored Pd-PtNPs. The spectrum of Pd3d and Pt4f were displayed in Fig. 2G and H. These results revealed that Cu@L-Glu/Pd-PtNPs composites were successfully synthesized.

3.3. Electrochemical characterization of the aptasensor

The cyclic voltammetry (CV) and electrochemical impedance spectroscopy (EIS) measurements were carried out to characterize the fabrication process of the aptasensor. The CV measurements were performed in a 5 mM $[Fe(CN)_6]^{3-/4-}$ solution. As shown in Fig. 3A, a pair of well-defined redox peaks was clearly observed for the bare GCE (curve a). After the modification of Au-PANI-Au (curve b), the peak current apparently increased owing to the good conductivity and electron transfer of Au-PANI-Au. After the modified electrode was incubated with AP, a dramatic decrease in peak current was observed (curve c), suggesting that the negatively charged phosphate backbone of the AP hindered the diffusion of $[Fe(CN)_6]^{3-/4-}$ toward the electrode surface. After blocking with MCH, a further decrease was observed on the peak current (curve d), due to the non-conductivity of MCH hindering electron transfer. Subsequently, When the hybridization reaction of ZEN aptamer and the Cu@L-Glu/Pd-PtNPs-CP, a dramatic increase in peak current was observed owing to the good conductivity and electron transfer of Pd-PtNPs (curve e). After ZEN (10 ng/mL) competed with bioconjugates for binding to ZEN aptamer, resulting in decreased the peak current (curve f).

The fabrication process of this aptasensor can also be monitored by the EIS. In the Nyquist diagram, the semicircle diameter at high frequencies equals the electron-transfer resistance, while the linear portion at low frequency represents the diffusion process. As shown in Fig. 3B, when Au-PANI-Au was coated onto the electrode, the resistance relatively decreased (curve b) compared to the bare GCE (curve a) because Au-PANI-Au was conductive to the transmission of electrons. Subsequently, When AP (curve c) and MCH (curve d) were successively attached to the electrode, the resistance increased significantly due to the non-conductive substances hindered the electron transfer.

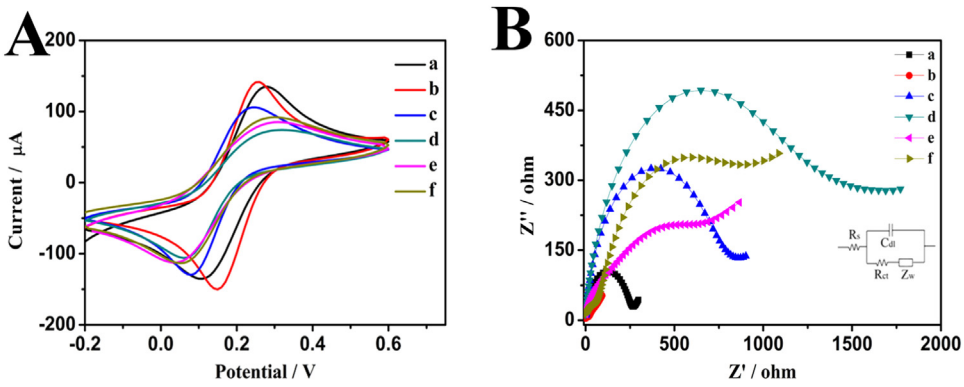

Fig. 3. (A) CV and (B) EIS characterization of electrodes at various stages of modification in a 5 mM $[Fe(CN)_6]^{3-/4-}$ solution: (a) bare GCE, (b) Au-PANI-Au/GCE, (c) AP/Au-PANI-Au/GCE, (d) MCH/AP/Au-PANI-Au/GCE, (e) Cu@L-Glu/Pd-PtNPs-CP MCH/AP/Au-PANI-Au/GCE, (f) ZEN/Cu@L-Glu/Pd-PtNPs-CP MCH/AP/Au-PANI-Au/GCE.

Subsequently, After the hybridization reaction of ZEN aptamer and the Cu@L-Glu/Pd-PtNPs-CP, a dramatic decrease in the resistance was observed (curve e), suggesting that the hybridization reaction was successful on the electrode surface. When ZEN (10 ng/mL) competed with bioconjugates for binding to ZEN aptamer, resulting in increased the resistance (curve f). The results of the EIS were in accordance with the CV. Additionally, the modification process of the electrode was investigated by AFM. More detailed data can be found in the Supplementary information (Fig. S3). All these results demonstrated the successful fabrication of the aptasensor.

3.4. Optimization of the experiment conditions

To achieve an optimal performance of the aptasensor, some experimental factors were taken into consideration, including the concentration of Au-PANI-Au, the concentration of AP, the immobilized time of AP, the concentration of Cu@L-Glu/Pd-PtNPs, the hybridization time between the AP and the CP, the concentration of H_2O_2 and interaction time of ZEN.

The concentration of Au-PANI-Au was investigated to improve the sensitivity of the aptasensor and provided a favorable platform for AP binding. As shown in Fig. S6A , the peak current change increased as the concentration of Au-PANI-Au increased. However, the peak current slightly declined after 2.4 mg/mL. This result can be caused by the excess amount of Au-PANI-Au blocked the electron transfer. Thus, 2.4 mg/mL of the Au-PANI-Au nanocomposites was chosen as the optimal concentration.

The concentration and the immobilized time of AP played important roles in aptasensor performance. As shown in Fig. S6B, the peak current change increased rapidly with increasing the concentration of AP from 1.0 μM to 2.0 μM and then began to level off. The maximum current change appeared at 2.0 μM. Therefore, 2.0 μM was selected as the optimal concentration of AP. The results of the immobilized time of AP in Fig. S6C showed that the peak current change increased with the immobilized time increasing from 0.5 to 1.5 h and reached the maximum value at 1.5 h. This indicated that the incubation of AP reached saturation after 1.5 h. Therefore, 2.0 μM of AP and 1.5 h were selected as the optimal concentration of AP and the optimal immobilized time.

The centration of Cu@L-Glu/Pd-PtNPs (Fig. S6D) and the hybridization time between the AP and the CP (Fig. S6E) were also notably important parameters. As shown in Fig. S6D, it was found that the current response increased significantly with increasing the concentration of Cu@L-Glu/Pd-PtNPs from 0.6 mg/mL to 1.0 mg/mL then reached saturation. Hence, 1.0 mg/mL of Cu@L-Glu/Pd-PtNPs was chosen throughout the subsequent experiments. As shown in Fig. S6E, the hybridization time was tested in the range from 1 to 3 h. The peak current change increased with increasing hybridization time from 1 to 2 h, and then began to level off. Accordingly, 2 h was selected as the optimal hybridization time.

Furthermore, the concentration of H_2O_2 (Fig. S6F) and the interaction time of ZEN (Fig. S6G) were critical factors for to achieving optimal electrochemical signal. In Fig. S6F, it was found that the current response increased significantly from 1.6 to 2.2 mol/L and then reached saturation. Hence, 2.2 mol/L of H_2O_2 was chosen throughout the subsequent experiments. In Fig. S6G, we have optimized the interaction time of ZEN (100 pg/mL) which was tested in the range from 1 to 3 h. The current response change decreased with increasing interaction time of ZEN from 1 to 2 h, and then began to level off. Accordingly, 2 h was selected as the optimal interaction time of ZEN.

3.5. The electrochemical behaviour of different nanomaterials for signal tags

PdNPs and PtNPs could enhance the performance of aptasensor by the catalysis of H_2O_2 and have an excellent biocompatibility with biomolecules (Li et al., 2017b). Bimetallic Pd-PtNPs had stronger catalytic activity to H_2O_2 than the single metal due to the synergetic effect of the second metal (Deng et al., 2012). In order to verify the mechanism of signal amplification strategy, different nanomaterials were compared by amperometric i-t curves. With showing in Fig. 4A, the Δcurrent of 200 μA were found when the Cu@L-Glu/PtNPs (curve a) was modified onto the electrode. The electrochemical signal further increased (curve b) when PdNPs were modified onto the Cu@L-Glu. Finally, when the Cu@L-Glu were functionalized with Pd-Pt NPs, the Δcurrent was obviously increased (curve c), which is attributed to the synergistic catalytic activities of Pd-Pt NPs. The experiment result confirmed that Cu@L-Glu/Pd-PtNPs had a better electrocatalytic ability than the other nanomaterials as a label. In addition, in Fig. S7. after ZEN addition (10 ng/mL), cyclic voltammograms of proposed electrode were also presented in the absence/presence of H_2O_2 and in the presence of H_2O_2, redox peaks can be clearly observed according to the curve b.

3.6. Performance of the aptasensor

Under the optimum assay conditions, the proposed aptasensor was incubated with a series of concentrations of ZEN. As seen in Fig. 4B, the current response decreased with an increasing concentration of the ZEN in 5 mL of PBS (0.1 M, pH 7.4). As shown in Fig. 4C, the current signal and the logarithm of the ZEN concentration exhibited a good linear relationship in the detection range from 1 fg/mL to 100 ng/mL, with a detection limit of 0.45 fg/mL (based on S/N = 3). The regression equation was $Y = -17.463 * \log C_{ZEN} + 317.79$ ($R^2 = 0.9972$), where Y is an amperometric i-t current increment, C_{ZEN} is the concentration of ZEN, and R^2 is the regression coefficient. In addition, Table S2 gives the linear range and detection limit of the current methods for ZEN detection. The proposed aptasensor shows a wider linear range and lower detection limit compared to the previously reported methods, indicating that the fabricated aptasensor exhibited a higher sensitivity.

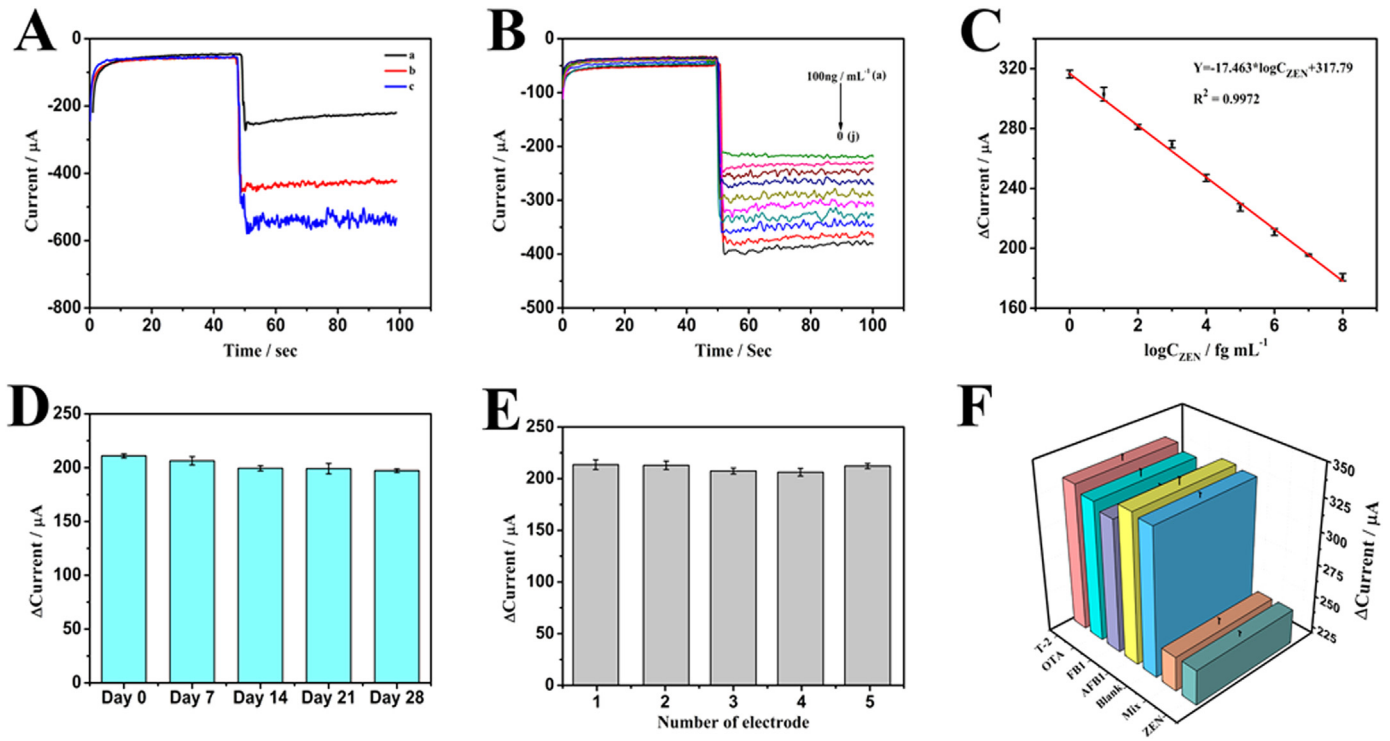

Fig. 4. (A) The Amperometric i-t curves of different nanomaterials (i-t curve was recorded at −0.4 V in pH 7.4 of PBS): (a) Cu@L-Glu/PtNPs, (b) Cu@L-Glu/PdNPs, (c) Cu@L-Glu/Pd-PtNPs; (B) i-t curve signals of the aptasensor for the determination of different concentrations of ZEN (i-t curve was recorded at −0.4 V in pH 7.4 of PBS): (a) 100 ng/mL, (b) 10 ng/mL, (c) 1 ng/mL, (d) 100 pg/mL, (e) 10 pg/mL, (f) 1 pg/mL, (g) 100 fg/mL, (h) 10 fg/mL, (i) 1 fg/mL; (j) 0 fg/mL. (C) The calibration curve of the aptasensor for different concentrations of ZEN (n = 3). (D) Stability of the aptasensor at 0 d, 7d, 14 d, 21 d, and 28 d. The ZEN concentration was 1 ng/mL (E) Reproducibility of five different electrodes modified with 1 ng/mL of ZEN. (F) Selectivity of the aptasensor for ZEN (10 pg/mL), several competing 5 interfering substances (T-2, OTA, FB1, AFB1) (1 ng/mL), a mixture (Mix) of the interfering substances (1 ng/mL) and ZEN (10 pg/mL) and zero analyte (Blank).

3.7. Stability, Reproducibility and Specificity of the aptasensor

To evaluate the stability of the aptasensor, the sensor was stored at 4 °C. After storage for 28 days, the final current change of sensor was 93.5% of its initial current response (Fig. 4D). The results revealed that the proposed aptasensor shows an acceptable stability. The reproducibility of the aptasensor were investigated by the measurement of the same concentration of ZEN (1 ng/mL) using five different electrodes (Fig. 4E). The relative standard deviation (RSD) of the aptasensor was found to be 1.59%, demonstrating its good reproducibility, which suggested the acceptable precision and reproducibility.

To evaluate the specificity of the constructed aptasensor, the effects of interfering substances (T-2, OTA, FB1, AFB1), blank control and the mixture (Mix) (consisted of the 1 ng/mL interference substances and the 10 ng/mL ZEN) were investigated, respectively. The results are shown in Fig. 4F, it was observed that the current response did not significantly decrease with the addition of interfering substances compare to that of the blank control, while a dramatic decrease in the current response was shown in the presence of the ZEN (1 ng/mL), and the mixture exhibited almost identical current response changes to those of the ZEN. These results suggested the satisfactory specificity of the proposed aptasensor.

3.8. Analysis of beer samples

To examine the analytical reliability and application of the aptasensor to real sample, the aptasensor was applied to beer samples spiked with 0.1, 10 and 1000 pg/mL ZEN. As seen as Table 1, the recovery of the three concentrations ranged from 92% to 105%, and the RSD of the three concentrations ranged from 0.79% to 1.61%, showing acceptable precision.

In addition, to examine the reliability of the aptasensor, analysis of three beer samples was performed via the developed method and ELISA method. As shown in Tables S3, the relative errors between the two methods were 9%, −7.76% and 3.68%, respectively, showing the consistency between the two analytical methods. These results demonstrated that the proposed aptasensor possessed good reliability for the detection of ZEN in food samples.

Table 1
Recovery of ZEN in beer samples (n = 3).

Sample	Added ZEN (pg/mL)	Founded ZEN (pg/mL)	RSD (%, n = 3)	Recovery (%, n = 3)
1	0.1	0.105	1.61	105.00
2	10	9.200	0.79	92.00
3	1000	943.377	1.27	94.34

4. Conclusion

In conclusion, a novel electrochemical aptasensor was proposed for ultrasensitive determination of ZEN by loading Pd-PtNPs nanoparticles on 3D sakura-shaped Cu@L-Glu MOCPs as label to amplify the current signal, which will promote the greater use of MOCPs in the biosensor field. Cu@L-Glu MOCPs were first successfully synthesized and Cu@L-Glu/Pd-PtNPs exhibited excellent electrocatalytic activity through catalyzing the reduction of H_2O_2, the detection signal could be significantly enhanced, the sensitivity of aptasensor could be further improved. Meanwhile, spherical Au-PANI-Au nanohybrids were first served as a sensor platform for immobilizing more aptamer. The developed aptasensor exhibited a low detection limit, a wide detection range, high specificity, excellent reproducibility and stability. Furthermore, the fabricated aptasensor was successfully applied to the detection of ZEN in beer samples with good recovery and agreed well

with the conventional ELISA method. Therefore, this could offer an ideal technology platform for the sensitive and accurate detection of ZEN or another small molecule toxin. However, the real samples in this study were not found, thus the next work is to collect real samples to further prove the feasibility of the aptasensor for the detection of ZEN.

Acknowledgement

We are grateful for the financial support from the Chongqing Technology Innovation and Application Demonstration (social and livelihood type general) Project, China (No. cstc2018jscx-msyb0008), the National Natural Science Foundation of China (No. 31271246; No. 81370403), the Chongqing Foundation and Advanced Research Project, China (No. CSTC2015jcyjBX0053) and Chongqing Graduate Scientific Research Innovation Project, China (CYS18208).

Declaration of interest statement

None.

Appendix A. Supporting information

Supplementary data associated with this article can be found in the online version at doi:10.1016/j.bios.2019.01.012.

References

Bennett, J.W., Klich, M., 2003. Clin. Microbiol. Rev. 16, 497–516.
Boomi, P., Prabu, H.G., Manisankar, P., Ravikumar, S., 2014. Appl. Surf. Sci. 300, 66–72.
Chen, F., Luan, C., Wang, L., Wang, S., Shao, L., 2017a. J. Sci. Food Agric. 97, 1805–1810.
Chen, Y., Li, Y., Yang, Y., Wu, F., Cao, J., Bai, L., 2017b. Microchim. Acta 184, 1801–1808.
Cho, E.J., Lee, J.W., Ellington, A.D., 2009. Annu Rev. Anal. Chem. (Palo Alto Calif.) 2, 241–264.
Deng, Y.-J., Tian, N., Zhou, Z.-Y., Huang, R., Liu, Z.-L., Xiao, J., Sun, S.-G., 2012. Chem. Sci. 3, 1157.
Du, J., Yue, R., Ren, F., Yao, Z., Jiang, F., Yang, P., Du, Y., 2014. Biosens. Bioelectron. 53, 220–224.
ElShafei, G.M.S., Yehia, F.Z., Dimitry, O.I.H., Badawi, A.M., Eshaq, G., 2010. Appl. Catal. B: Environ. 99, 242–247.
Fan, H., Guo, Z., Gao, L., Zhang, Y., Fan, D., Ji, G., Du, B., Wei, Q., 2015. Biosens. Bioelectron. 64, 51–56.
Fang, Y., Wang, S., Liu, Y., Xu, Z., Zhang, K., Guo, Y., 2018. Biosens. Bioelectron. 110, 44–51.
Fu, Y., Li, P., Bu, L., Wang, T., Xie, Q., Chen, J., Yao, S., 2011. Anal. Chem. 83, 6511–6517.
Ghali, R., Hmaissia-khlifa, K., Ghorbel, H., Maaroufi, K., Hedili, A., 2008. Food Control 19, 921–924.
Haiss, W., Thanh, N.T.K., Aveyard, J., Fernig, D.G., 2007. Anal. Chem. 79, 4215–4221.
Hanifehpour, Y., Safarifard, V., Morsali, A., Mirtamizdoust, B., Joo, S.W., 2015. Ultrason. Sonochem. 23, 282–288.
Hervas, M., Lopez, M.A., Escarpa, A., 2009. Anal. Chim. Acta 653, 167–172.
Hervas, M., Lopez, M.A., Escarpa, A., 2010. Biosens. Bioelectron. 25, 1755–1760.
Joshi, R.K., Schneider, J.J., 2012. Chem. Soc. Rev. 41, 5285–5312.
Kong, Q., Wang, Y., Zhang, L., Xu, C., Yu, J., 2018. Biosens. Bioelectron. 110, 58–64.
Kong, W., Xiao, C., Ying, G., Liu, X., Zhao, X., Wang, R., Wan, L., Yang, M., 2017. Biosens. Bioelectron. 94, 420–428.
Lee, S.W., Cheon, S.A., Kim, M.I., Park, T.J., 2015. J. Nanobiotechnol. 13, 54.
Li, J.F., Zhang, Y.J., Ding, S.Y., Panneerselvam, R., Tian, Z.Q., 2017a. Chem. Rev. 117, 5002–5069.
Li, M., Wang, P., Li, F., Chu, Q., Li, Y., Dong, Y., 2017b. Biosens. Bioelectron. 87, 752–759.
Lin, H., Luan, J., Wang, X., Zhang, J., Liu, G., Tian, A., 2014. RSC Adv. 4, 62430.
Liu, J., Hu, Y., Zhu, G., Zhou, X., Jia, L., Zhang, T., 2014. J. Agric. Food Chem. 62, 8325–8332.
Ma, Z., Moulton, B., 2011. Coord. Chem. Rev. 255, 1623–1641.
Mahmoudi, G., Morsali, A., 2009. Inorg. Chim. Acta 362, 3238–3246.
Masoomi, M.Y., Morsali, A., 2013. RSC Adv. 3, 19191.
Njumbe Ediage, E., Van Poucke, C., De Saeger, S., 2015. Food Chem. 177, 397–404.
Pu, F., Liu, X., Xu, B., Ren, J., Qu, X., 2012. Chemistry 18, 4322–4328.
Qin, Y., Chao, L., Yuan, J., Liu, Y., Chu, F., Kong, Y., Tao, Y., Liu, M., 2016. Chem. Commun. (Camb.) 52, 382–385.
Richard, J.L., 2007. Int. J. Food Microbiol. 119, 3–10.
Sajanlal, P.R., Sreeprasad, T.S., Nair, A.S., Pradeep, T., 2008. Langmuir 24, 4607–4614.
Schmidt, K.S., Borkowski, S., Kurreck, J., Stephens, A.W., Bald, R., Hecht, M., Friebe, M., Dinkelborg, L., Erdmann, V.A., 2004. Nucleic Acids Res. 32, 5757–5765.
Schneider, E.P., Dickert, K.J., 1994. J. Agromed. 1, 19–37.
Singha, S.S., Mondal, S., Bhattacharya, T.S., Das, L., Sen, K., Satpati, B., Das, K., Singha, A., 2018. Biosens. Bioelectron. 119, 10–17.
Singhal, C., Pundir, C.S., Narang, J., 2017. Biosens. Bioelectron. 97, 75–82.
Wang, C., Zheng, M., Lin, W., 2011a. J. Phys. Chem. Lett. 2, 1701–1709.
Wang, X., Shen, Y., Xie, A., Li, S., Cai, Y., Wang, Y., Shu, H., 2011b. Biosens. Bioelectron. 26, 3063–3067.
Wei, Q., Zhao, Y., Xu, C., Wu, D., Cai, Y., He, J., Li, H., Du, B., Yang, M., 2011. Biosens. Bioelectron. 26, 3714–3718.
Wu, J., He, J., Zhang, C., Chen, J., Niu, Y., Yuan, Q., Yu, C., 2018. Biosens. Bioelectron. 102, 403–410.
Xu, W., Qing, Y., Chen, S., Chen, J., Qin, Z., Qiu, J., Li, C., 2017. Microchim. Acta 184, 3339–3347.
Yan, Z., Wang, F., Deng, P., Wang, Y., Cai, K., Chen, Y., Wang, Z., Liu, Y., 2018. Biosens. Bioelectron. 109, 132–138.
Zaied, C., Zouaoui, N., Bacha, H., Abid, S., 2012. Food Control 25, 773–777.
Zhang, C., He, J., Zhang, Y., Chen, J., Zhao, Y., Niu, Y., Yu, C., 2018a. Biosens. Bioelectron. 102, 94–100.
Zhang, F., Liu, B., Sheng, W., Zhang, Y., Liu, Q., Li, S., Wang, S., 2018b. Food Chem. 255, 421–428.
Zhang, X., Eremin, S.A., Wen, K., Yu, X., Li, C., Ke, Y., Jiang, H., Shen, J., Wang, Z., 2017. J. Agric. Food Chem. 65, 2240–2247.
Zhou, B., Liang, L.-M., Yao, J., 2014. J. Solid State Chem. 215, 109–113.
Zinedine, A., Soriano, J.M., Molto, J.C., Manes, J., 2007. Food Chem. Toxicol. 45, 1–18.